Disease Models & Mechanisms 4, 763-776 (2011) doi:10.1242/dmm.007625

RESEARCH ARTICLE

The *feelgood* mutation in zebrafish dysregulates COPII-dependent secretion of select extracellular matrix proteins in skeletal morphogenesis

David B. Melville[1,2], Mercedes Montero-Balaguer[1], Daniel S. Levic[1,2], Kevin Bradley[1], Jeffrey R. Smith[1], Antonis K. Hatzopoulos[3] and Ela W. Knapik[1,2,*]

SUMMARY

Craniofacial and skeletal dysmorphologies account for the majority of birth defects. A number of the disease phenotypes have been attributed to abnormal synthesis, maintenance and composition of extracellular matrix (ECM), yet the molecular and cellular mechanisms causing these ECM defects remain poorly understood. The zebrafish *feelgood* mutant manifests a severely malformed head skeleton and shortened body length due to defects in the maturation stage of chondrocyte development. In vivo analyses reveal a backlog of type II and type IV collagens in rough endoplasmic reticulum (ER) similar to those found in coat protein II complex (COPII)-deficient cells. The *feelgood* mutation hinders collagen deposition in the ECM, but trafficking of small cargos and other large ECM proteins such as laminin to the extracellular space is unaffected. We demonstrate that the zebrafish *feelgood* mutation causes a single amino acid substitution within the DNA-binding domain of transcription factor Creb3l2. We show that Creb3l2 selectively regulates the expression of genes encoding distinct COPII proteins (*sec23a*, *sec23b* and *sec24d*) but find no evidence for its regulation of *sec24c* expression. Moreover, we did not detect activation of ER stress response genes despite intracellular accumulation of collagen and prominent skeletal defects. Promoter trans-activation assays show that the Creb3l2 *feelgood* variant is a hypomorphic allele that retains approximately 50% of its transcriptional activity. Transgenic rescue experiments of the *feelgood* phenotype restore craniofacial development, illustrating that a precise level of Creb3l2 transcriptional activity is essential for skeletogenesis. Our results indicate that Creb3l2 modulates the availability of COPII machinery in a tissue- and cargo-specific manner. These findings could lead to a better understanding of the etiology of human craniofacial and skeletal birth defects as well as adult-onset diseases that are linked to dysregulated ECM deposition, such as arthritis, fibrosis or osteoporosis.

INTRODUCTION

Extracellular matrix (ECM) serves as a structural scaffold and a reservoir for biologically active molecules (Hynes, 2009). Cartilage formation and skeletal morphogenesis depend on timely and abundant deposition of ECM proteins (DeLise et al., 2000). Failure to produce adequate mature ECM or form proper collagen fibers can lead to many developmental defects and diseases, such as osteogenesis imperfecta – which is typically characterized by fragile bones, scoliosis, short stature, hearing loss and teeth defects (Rauch and Glorieux, 2004). In adults, failure to maintain the ECM of the bone can lead to degenerative diseases such as osteoporosis, a debilitating condition characterized by a loss in bone density. Similarly, interstitial fibrosis leading to organ failure after injury, or pathological conditions in aging patients such as arthritis, have been associated with dysregulated protein secretion (Trojanowska et al., 1998; Heinegård and Saxne, 2011; Goldring and Goldring, 2010; Goldring and Goldring, 2007; Löppönen et al., 2004).

ECM proteins depend on the secretory machinery for transport to the extracellular space. The initial step of protein trafficking occurs when proteins leave the site of synthesis in the endoplasmic reticulum (ER) and are transported to the Golgi. This step is primarily conducted by coat protein II complex (COPII) vesicular carriers (Barlowe et al., 1994; Dancourt and Barlowe, 2010; Miller and Barlowe, 2010). The COPII complex is recruited to the ER membrane by the Sar1 GTPase and consists of an inner coat of Sec23-Sec24 heterodimers and an outer coat of Sec13-Sec31 proteins. Vertebrate genomes carry two highly similar paralogs of Sec23 (Sec23A and Sec23B) and four paralogs of Sec24 (Sec24A, Sec24B, Sec24C and Sec24D). Sec23 paralogs act as GTPase-activating proteins for Sar1, whereas Sec24 proteins play a role in cargo sorting (Wendeler et al., 2007).

Mutations in genes encoding COPII components have been implicated in a variety of human disorders, with defects in closely related paralogs causing widely different phenotypes (Boyadjiev et al., 2006; Schwarz et al., 2009; Aridor and Hannan, 2002; Routledge et al., 2010). For example, mutations in SEC23B lead to congenital dyserythropoietic anemia type II (CDAII), a disease characterized by ineffective erythropoiesis, bi- and multinucleated erythroblasts, and hypoglycosylation of red blood cell membrane proteins (Bianchi et al., 2009; Schwarz et al., 2009). By contrast, a point mutation in SEC23A leads to cranio-lenticulo-sutural dysplasia (CLSD), the distinctive marks of which include craniofacial skeleton malformations and short stature (Boyadjiev et al., 2006). Zebrafish

[1]Department of Medicine, Division of Genetic Medicine, Vanderbilt University Medical Center, Nashville, TN 37232, USA
[2]Department of Cell and Developmental Biology, Vanderbilt University Medical Center, Nashville, TN 37232, USA
[3]Department of Medicine, Division of Cardiovascular Medicine, Vanderbilt University Medical Center, Nashville, TN 37232, USA
*Author for correspondence (ela.knapik@vanderbilt.edu)

Received 12 January 2011; Accepted 14 May 2011

crusher (*sec23a*) mutant and *sec23b* morphant embryos present phenotypes that are similar to the corresponding human diseases, establishing zebrafish as a model system to study the molecular and cellular bases of COPII deficiencies (Lang et al., 2006; Schwarz et al., 2009).

Further establishing the paralog-specific defects seen with loss of COPII components, another zebrafish mutant, *bulldog* (*sec24d*), was recently described (Sarmah et al., 2010). Loss of Sec24D activity in zebrafish also results in craniofacial defects, whereas Sec24C morphants undergo normal development of head skeletal structures. Loss of *bulldog* (*sec24d*) does not prevent neural crest migration, formation of pharyngeal condensations, or proliferation of chondrocytes, but hinders normal maturation of highly secretory chondrocytes. Strikingly, the combined loss of Sec24C and Sec24D results in neural crest migration and condensation deficits, indicating that Sec24D activity is essential for chondrocyte maturation, but Sec24C or Sec24D compensate for each other in early stages of cartilage development (Melville and Knapik, 2011).

Considering the high levels of similarity between COPII paralogs and the basic cellular function that they perform, these findings suggest that COPII-dependent anterograde protein transport is a highly regulated process both during development and under physiological conditions in adulthood, and therefore is likely to be a factor in many more diseases than those already characterized. However, the mechanisms of this regulation are still in the early stages of being understood.

Forward genetic screens in model organisms, such as the one that isolated the *crusher* and *bulldog* mutants (Neuhauss et al., 1996), provide an unbiased approach to discover physiologically relevant mutations that affect skeletal development. Here, we have characterized the *feelgood* (*fel*^{m662}) mutant, which belongs to the same phenotypic series as *crusher* and *bulldog*. We found that the *feelgood* mutation disrupts head skeleton and notochord development through loss of secretory capacity. The *feelgood* defect specifically disrupts collagen trafficking, thus decoupling its transport from that of other secretory and ECM proteins. We show that the *feelgood* phenotype is caused by a missense mutation in the DNA-binding domain of the transcription factor cAMP responsive element binding protein 3-like 2 (Creb3l2). We provide the first evidence of paralog-specific regulation of COPII components by showing that loss of Creb3l2 activity decreases the expression of *sec23a*, *sec23b* and *sec24d*, but not of *sec24c*. Our results suggest that Creb3l2 acts primarily as a transcriptional regulator of specific COPII components, establishing a mechanism that enables cell-type, cargo- and tissue-specific functions of COPII vesicles during development and providing a possible mechanism for the diverse disease manifestations caused by loss of COPII. Our results also suggest that skeletal development is highly sensitive to the level of Creb3l2 activity in vivo and advance Creb3l2 as a candidate cause for skeletal diseases of unknown genetic origin.

RESULTS

The zebrafish *feelgood* mutation causes craniofacial defects

The primary features of the *feelgood* phenotype include a reduced lower jaw, shortened body length, and compact head, trunk and tail as measured from the posterior edge of the ear capsule (Fig. 1A,B, white arrow) to the tip of the tail (Fig. 1A-D). Alcian blue staining (Fig. 1E-F′) reveals that all cartilage elements of the head skeleton are present in *feelgood* mutants, but they are shortened and malformed, including abnormal curvature of the Meckel's and ceratohyal cartilages, and failure of the Meckel's cartilage to taper towards the anterior end (Fig. 1F′).

Histological analysis by toluidine blue staining (Fig. 1G,H) shows reduced ECM surrounding the chondrocytes and tightly packed nuclei in *feelgood* mutants (Fig. 1H, arrow). Furthermore, the overall pattern of chondroblast intercalations and stacking is disrupted. These features are shared with the head skeleton defects observed in the *crusher* and *bulldog* mutants (Lang et al., 2006; Sarmah et al., 2010; Melville and Knapik, 2011).

Type II collagen trafficking is disrupted in *feelgood* mutant chondrocytes

To investigate whether abnormal cartilage shape in *feelgood* mutants is associated with trafficking deficits of ECM proteins,

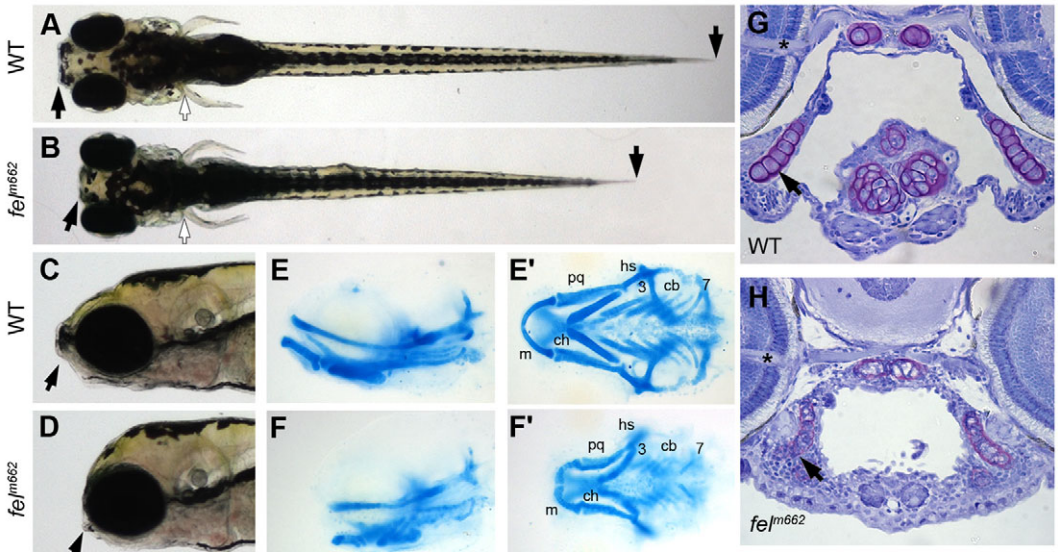

Fig. 1. The *feelgood* mutation affects craniofacial skeletal development. (A-D) Live images of wild-type (WT) and *feelgood* (*fel*^{m662}) embryos at 5 dpf. Arrows indicate reduced length of head and trunk in dorsal (A,B) and lateral (C,D) views. (E-F′) Alcian blue staining of cartilage elements in head skeleton in lateral (E,F) and ventral (E′,F′) views. cb, ceratobranchials 3-7; ch, ceratohyal; hs, hyosymplectic; m, Meckel's cartilage; pq, palatoquadrate. (G,H) Toluidine blue staining of transverse sections of the jaw at the level of the optic nerve (asterisk). Nuclei stain blue, whereas ECM stains purple. Arrow indicates tightly packed nuclei in *feelgood* mutants.

as is the case with *crusher* and *bulldog*, we examined the cellular distribution of Collagen2α1 (Col2α1) in chondrocytes at 80 hpf, the earliest stage at which *feelgood* mutants can be clearly identified, and in 5-dpf embryos. In addition, we compared collagen trafficking to bulk transport of secreted glycoproteins by staining N-acetylglucosamine or sialic acid residues with wheat germ agglutinin (WGA).

In 80-hpf wild-type embryos, both Col2α1 and WGA labeling was primarily localized to the extracellular space (Fig. 2A-A″), with small clusters of intracellular staining probably representing the Golgi apparatus (Allen et al., 1989). In *feelgood* mutants, WGA staining also appeared in the extracellular space and the Golgi apparatus (Fig. 2B), suggesting that *feelgood* mutants traffic the bulk of WGA-binding glycoproteins at close to normal levels. By contrast, immunofluorescence staining in *feelgood* mutants revealed deposition of Col2α1 to the extracellular space but also accumulation in cytosolic vesicle-like structures, which were larger and denser than the corresponding intracellular compartments in wild types (Fig. 2A′,B′). By 5 dpf, *feelgood* and wild-type WGA staining patterns were similar (Fig. 2C,D), whereas the intracellular type II collagen accumulation in *feelgood* chondrocytes had increased (Fig. 2C′,D′).

To identify the intracellular localization of protein buildup, we used transmission electron microscopy (TEM). TEM images showed that chondrocytes were stacked in a regular fashion in wild-type embryos (Fig. 2E,I), whereas, in *feelgood*, chondrocytes had a round morphology and were irregularly spaced, suggesting stacking defects (Fig. 2G,K). At this stage, rough ER, identified as ribosome dotted membranes, was severely, but not uniformly, distended in *feelgood* mutants (Fig. 2F,H). By 5 dpf, chondrocytes in wild-types had become hypertrophic, lacking dense rough ER (Fig. 2I,J). Conversely, chondrocytes in *feelgood* seem to be arrested at earlier stages of

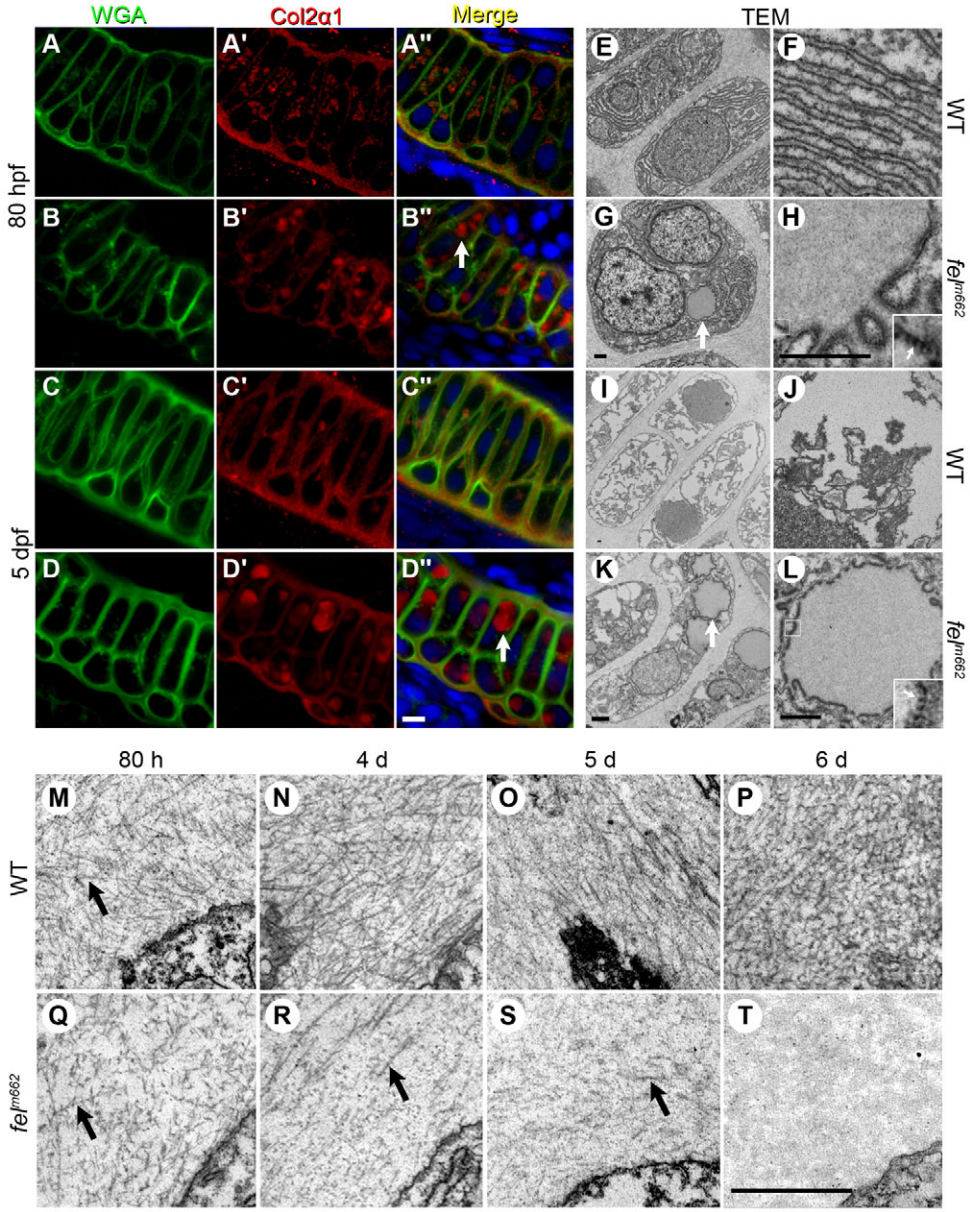

Fig. 2. Protein trafficking is disrupted in *feelgood* mutants. (A-D″) Immunostaining of WGA (A-D) and Col2α1 (A′-D′) in the Meckel's cartilage of 80-hpf (A-B″) and 5-dpf (C-D″) wild-type (WT; A-A″, C-C″) and *feelgood*. (B-B″, D-D″) embryos. Arrows in merged images indicate aberrant intracellular collagen localization in *feelgood*. Scale bar: 5 µm. (E-L) TEM images of 80-hpf (E-H) and 5-dpf (I-L) WT and *feelgood* chondrocytes. Arrows indicate distended ER membranes in *feelgood* cells. (M-T) TEM images of collagen fibrils in the extracellular space of *feelgood* mutants and WT siblings at 80 hpf and 4, 5 and 6 dpf. Arrows point to representative individual collagen fibrils. Scale bar: 1 µm.

maturation, containing large vacuoles of distended ER membranes filled with electron dense material (Fig. 2K,L).

Taken together, these data indicate that the jaw deformity in *feelgood* mutants is probably a consequence of abnormal collagen secretion and continuous intracellular protein buildup, leading to a progressively more severe phenotype. They also suggest that the maturation of *feelgood* chondrocytes towards a hypertrophic state is delayed or stalled, subsequent to insufficient matrix deposition, which is known to cause deficits in matrix-mediated intracellular signaling (Hickok et al., 1998).

Cartilage matrix is progressively lost in *feelgood* mutants

Cartilage matrix is continuously turned over during development and tissue homeostasis. Maintenance of cartilage matrix requires synchronization of a number of cellular functions, including coordinated protein secretion, cell-matrix signaling and protein degradation. To query how the intracellular defect in collagen transport affects ECM formation, we compared the ultrastructure of cartilage matrix in TEM images of wild-type and *feelgood* embryos (Fig. 2M-T). In this analysis, we examined tissue sections from the earliest stage at which we can morphologically distinguish the *feelgood* phenotype (80 hpf), followed by analyses on days 4, 5 and 6 of development. We found that *feelgood* mutant matrix at 80 hpf contains collagen fibrils (Fig. 2Q), suggesting that collagen is successfully synthesized and secreted by chondrocytes at the initial stages of chondrogenesis. However, as collagen fibrils grow progressively denser in wild-type cartilage (Fig. 2M-P), ECM matrix in *feelgood* becomes gradually more sparse and devoid of collagen bundles with an almost complete absence of organized fibrils by 6 dpf (Fig. 2Q-T).

Thus, cartilage collagen is being initially secreted by *feelgood* chondrocytes, albeit at lower levels than in wild types. However, the typical increase in matrix secretion during cartilage differentiation at the 4 dpf stage is absent, suggesting that *feelgood* is required for sustained, high-volume traffic of ECM proteins.

Notochord sheath formation, but not secretion of glycosaminoglycans, is disrupted in *feelgood* mutants

feelgood mutant embryos are shorter than wild types, pointing to disrupted notochord development. In zebrafish embryos, the notochord functions as a hydrostatic skeleton, the mechanical properties of which depend on an external fibrous sheath – which consists primarily of collagen and laminin matrix – and numerous internal vacuoles in notochord sheath cells – which enclose secreted glycosaminoglycans (GAGs) with high affinity for water (Scott and Stemple, 2005; Adams et al., 1990). Both of these biomechanical components exert the appropriate notochord stiffness that is essential for embryo lengthening and maintenance of straight posture.

To determine the secretory status of GAG proteins in the notochord sheath, we used WGA staining. The results show that, at 28 hpf, WGA-stained proteins are trafficked through the notochord sheath cells of *feelgood* embryos to the extracellular space (Fig. 3A,B,E,F). The major components of the notochord sheath are type II and type IV collagen fibrils that are interlinked with laminins, nidogen and fibulins: the typical components of basement membranes (Timpl and Brown, 1996). We analyzed the secretory status of the type II and type IV collagens by immunofluorescence and found that both are abnormally localized within large vesicle-like structures similar to those seen in the craniofacial cartilage (Fig. 3C-F,I-L).

To determine whether secretory defects extend to other ECM proteins, we analyzed the localization of laminin in the notochord and somitic boundaries, and we detected no deficits in deposition in *feelgood* embryos compared with wild types (Fig. 3M,N, and data not shown). Histological analysis of transverse sections stained with toluidine blue in 80-hpf embryos further corroborated the findings at earlier stages and revealed a less robust notochord sheath in *feelgood* compared with wild types (Fig. 3O-R). These data suggest that the transport of GAGs to internal vacuoles, as well as the secretion of WGA-binding glycoproteins and laminin, is not disrupted in *feelgood* mutants. By contrast, *feelgood* specifically affects the secretion of type II and type IV collagens, resulting in an overall weaker and smaller fibrous sheath surrounding the notochord, which is consistent with the shorter body length of *feelgood* embryos.

To further assess the secretory capability of the *feelgood* embryos, we analyzed total protein extracts from 4-dpf embryos on western blots probed with antibodies against type II collagen. We found an increase in unprocessed procollagen, consistent with a trafficking defect (Fig. 3S).

Furthermore, immunoblot analysis of protein extracts using N-cadherin antibody found that *feelgood* N-cadherin was resistant to endoglycosidase H (Endo H; which cleaves mannose-rich structures) but sensitive to PNGase F (which cleaves high-mannose as well as complex-type N-glycans). This indicates that N-cadherin is normally processed in *feelgood* mutants and progresses along the intracellular secretory pathway, consistent with its plasma membrane localization in *feelgood* chondroblasts (Fig. 3T, and data not shown).

The *feelgood* mutation affects melanosome maturation

To test whether the *feelgood* phenotype affects other cell types that are characterized by high levels of protein trafficking, including those that do not secrete collagen, we analyzed pigment cell maturation. This process involves intensive protein transport during the biogenesis of melanosomes, a set of morphologically and functionally unique organelles that accumulate melanin and translocate within melanocytes in response to pigment modulating stimuli (Marks and Seabra, 2001). Our results show that, although pigment appears normal, the ability of *feelgood* melanocytes to respond to stimuli is disrupted (Fig. 4A-D). Specifically, when stress was induced by a low concentration of the melanotoxic 4-hydroxyanisole (Riley et al., 1975), melanosomes in wild-type pigment cells responded by aggregating into small dense structures as previously described (Logan et al., 2006). However, in *feelgood* embryos, melanosomes failed to aggregate when stimulated with 4-hydroxyanisole and melanosome concentrating hormone (Fig. 4C,D, and data not shown).

To gain insight on pigment aggregation phenotype, we compared the ultrastructural characteristics of melanosomes between wild-type and *feelgood* fish (Fig. 4E-G). TEM images revealed that, in wild types, melanosomes mature to flattened, oval shape structures, whereas, in *feelgood* mutants, they appear uniform in size and circular in shape (Fig. 4F,G). This phenotype is similar to the melanosome maturation defects observed in the murine and

zebrafish *silver* mutants (Theos et al., 2006; Schonthaler et al., 2005). The *silver* phenotype is caused by failure to transport Pmel17, a structural protein that is required to maintain the oval shape of melanosomes, across the ER membrane (Theos et al., 2006).

Taken together, these results show that *feelgood* disrupts normal melanosome maturation in melanocytes. Thus, it appears that *feelgood* has critical functions in distinct cell types and not only in collagen-producing cells.

The *feelgood* mutation disrupts the *creb3l2* locus

The similarities between the *feelgood* phenotype and the phenotypes of the *crusher* and *bulldog* mutants, which abolish the function of two key COPII components, suggested that the *feelgood* locus encodes a protein participating in COPII-mediated transport. To identify the chromosomal location of the *feelgood* mutation, we utilized a positional cloning strategy. We genotyped fish from an F2 intercross and used the zebrafish genetic linkage map (Knapik

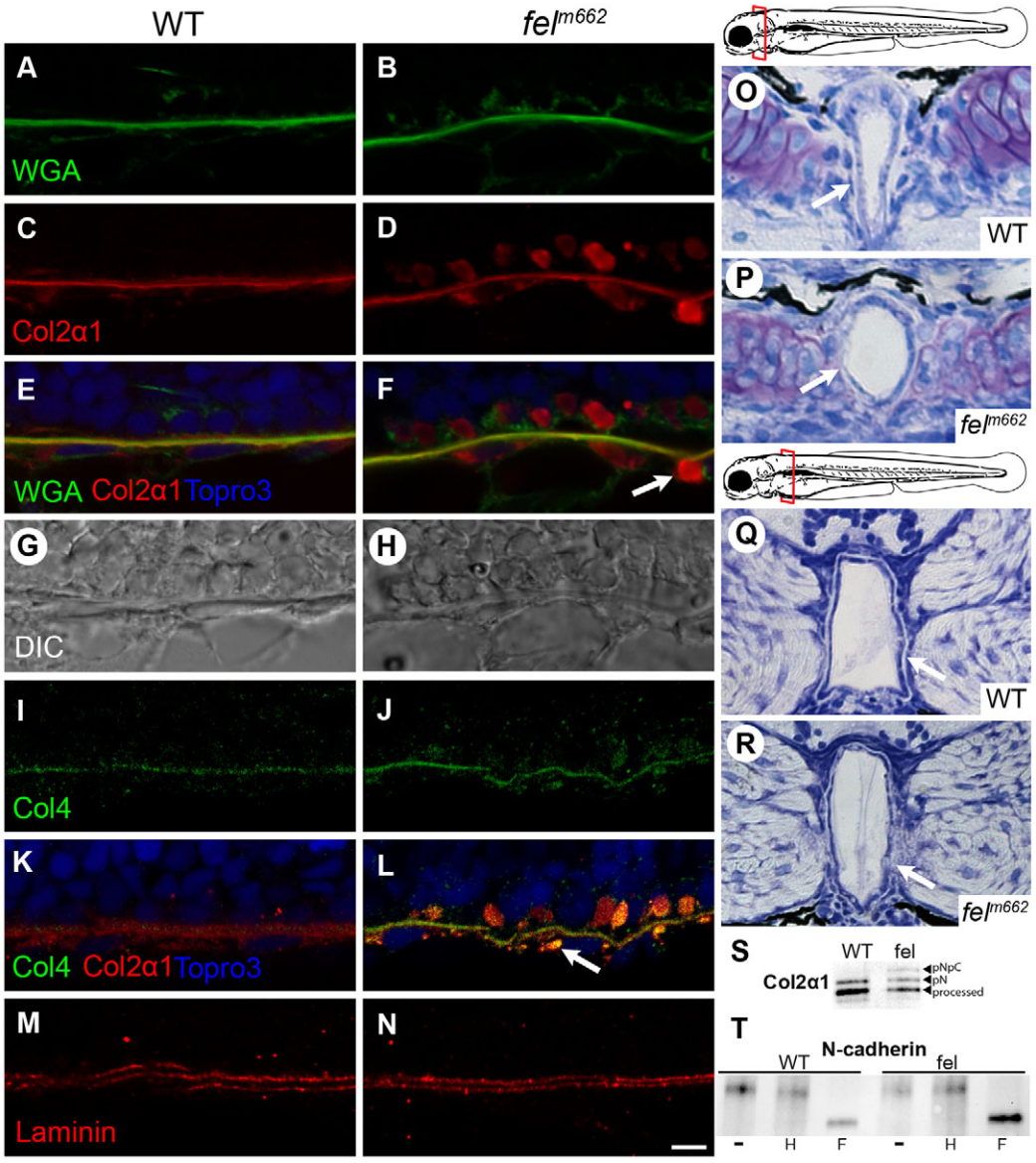

Fig. 3. Collagen trafficking is preferentially disrupted in *feelgood* mutants, leading to notochord defects. (A-F) Immunofluorescence of WGA, Col2α1 and merged images of 15-µm sagittal sections of the notochord of 28-hpf embryos. Arrow indicates vesicle-like collagen staining outside the notochord sheath. (G,H) DIC images of the corresponding sections in A-F. (I-N) Immunofluorescence of type-IV and type-II collagen (I-L) and laminin (M,N) in 15-µm sagittal sections of the notochord at 28 hpf. Scale bar: 5 µm. (O-R) Toluidine blue staining of transverse sections through the notochord at the level of the posterior parachordal plate (O,P) and posterior medulla oblongata (Q,R) in 80-hpf embryos. Schematic diagrams mark the plane of the corresponding sections. Arrows indicate the less robust notochord sheath in *feelgood* compared with wild types. (S) Immunoblot analysis of type II collagen processing. Molecular forms are indicated as: processed, the fully processed form; pN, pN-collagen II; pNpC, unprocessed procollagen II. (T) EndoH sensitivity assay for N-cadherin. Embryo lysates were either untreated (–) or treated with either EndoH (H) or PNGase F (F) before immunoblotting for N-cadherin.

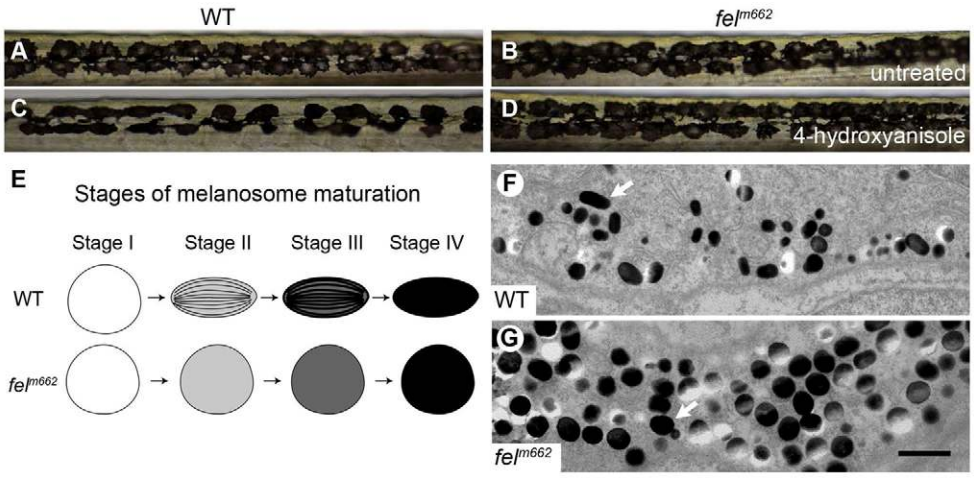

Fig. 4. Melanophore development is disrupted in *feelgood* mutants. (A-D) Live image of melanophores in the trunk of 6-dpf wild-type (WT) and *feelgood* mutants in untreated (A,B) and 0.5 μg/ml 4-hydroxyanisole treated (C,D) embryos. (E) Summary drawing of the stages of melanosome maturation comparing normal and *feelgood* melanocytes. (F,G) TEM images of 5-dpf melanosomes. Arrows point to a mature melanosome in WT (F), and a round, dark, stage IV melanosome in *feelgood* (G). Scale bar: 1 μm.

et al., 1998; Bradley et al., 2007) to establish that the *feelgood* mutation is located in a 5.2 cM region on the proximal arm of chromosome 4 (Fig. 5A). We then built a physical map of the critical region between these markers using the Zv7 genomic assembly to obtain contigs, and bridged the gaps between contigs using BAC information from the Zebrafish Genome Fingerprinting Project and sequences from the Ensembl trace repository. We confirmed the accuracy of our physical map by developing simple sequence length polymorphism (SSLP) markers from BAC or contig sequences and counting recombination events in a 2510 meioses F2 map cross. Finally, we restricted the critical interval to a 58 kb region flanked proximally by a marker within an intron of the *creb3l2* gene, and distally by a marker in intron 20 of the *diacylglycerol kinase, iota* (*dgki*) gene. No other known genes are present in the critical region (Fig. 5A).

Sequencing of the coding region of the two candidate genes revealed a single C>G transversion at base pair 1128 of the *creb3l2* gene that results in an N301K missense mutation (Fig. 5B,C). The Creb3l2 protein contains a basic leucine zipper domain consisting of a basic motif that mediates sequence-specific DNA binding, a leucine zipper motif that facilitates protein dimerization (Vinson et al., 1989; Hope and Struhl, 1987) and a single-pass transmembrane domain preceding a Site-1 protease (S1P) recognition site (Fig. 5B). The *feelgood* mutation is located within the DNA-binding basic motif of Creb3l2, in a segment that is conserved from *Caenorhabditis elegans* to human (Fig. 5D). *Creb3l2* belongs to a family of five paralogs that are highly conserved among vertebrate species, including zebrafish. Phylogenetic analysis showed that zebrafish *creb3l2* is the most similar zebrafish paralog to human *CREB3L2* (supplementary material Fig. S1).

To determine whether loss of Creb3l2 function is responsible for the *feelgood* phenotype, we designed a Tol2-based rescue construct (Kwan et al., 2007) containing wild-type *bactin2:creb3l2-mCherry* that was injected into *feelgood* mutants to create chimeric transgenic fish overexpressing wild-type and mutant proteins (Fig. 5E). Approximately 1/4 of the injected *feelgood* mutant embryos showed a partial rescue of the *feelgood* phenotype as indicated by the longer jaw, which protrudes past the eyes, and the presence of cartilage elements whose shape closely resembles that of wild types (Fig. 5F,H). A similar construct that contained the putative *feelgood* (N301K) mutation in *creb3l2* failed to rescue, indicating that the N301K substitution disturbs *creb3l2* function and accounts for the *feelgood* mutant phenotype (Fig. 5G,I,J).

creb3l2 is expressed in the developing pharyngeal arches

To determine whether the spatiotemporal expression pattern of *creb3l2* during development matches the structures that are most affected in *feelgood* mutants, we analyzed RNA samples by reverse transcriptase (RT)-PCR and embryos by whole mount in situ hybridization at sequential developmental time points. RNA analysis revealed that *creb3l2* mRNA is maternally deposited and that the amount of transcript decreases after the onset of zygotic transcription at the mid-blastula transition. As development proceeds, *creb3l2* is steadily expressed throughout morphogenesis, with the highest level at 4 dpf (supplementary material Fig. S2A). Probing embryos by in situ hybridization with digoxigenin-labeled *creb3l2* riboprobes showed that *creb3l2* is ubiquitously expressed during early development (supplementary material Fig. S2B). By 36 hpf, *creb3l2* RNA became primarily localized to the developing jaw, pectoral fins and the otic capsule (supplementary material Fig. S2C), and expression is maintained throughout jaw development (supplementary material Fig. S2D-E′). These results show that Creb3l2 is highly expressed in tissues that show developmental deficits in *feelgood* embryos, consistent with a direct role for Creb3l2 in craniofacial morphogenesis.

creb3l2 knockdown phenocopies the *feelgood* defects

The *feelgood* mutation most probably disrupts the DNA-binding ability of Creb3l2, resulting in partial or complete loss of function. To determine whether *feelgood* is a null or a hypomorphic allele, we knocked down Creb3l2 protein using two morpholinos (MO-1 and MO-2; Fig. 6A). Although both produced similar results, MO-2, which straddles the exon 4 splice acceptor site of the *creb3l2* gene locus in order to disrupt transcript processing, was more effective. MO-2 is predicted to cause a frame shift that generates a stop codon at amino acid 209 and leads to a truncated peptide lacking all characterized functional domains (Fig. 6A). Injection of MO-2 resulted in depletion of the spliced *creb3l2* transcript as evaluated by RT-PCR (Fig. 6A). The observed MO-2 phenotype is similar to that of *feelgood*, although the morphant defects are more

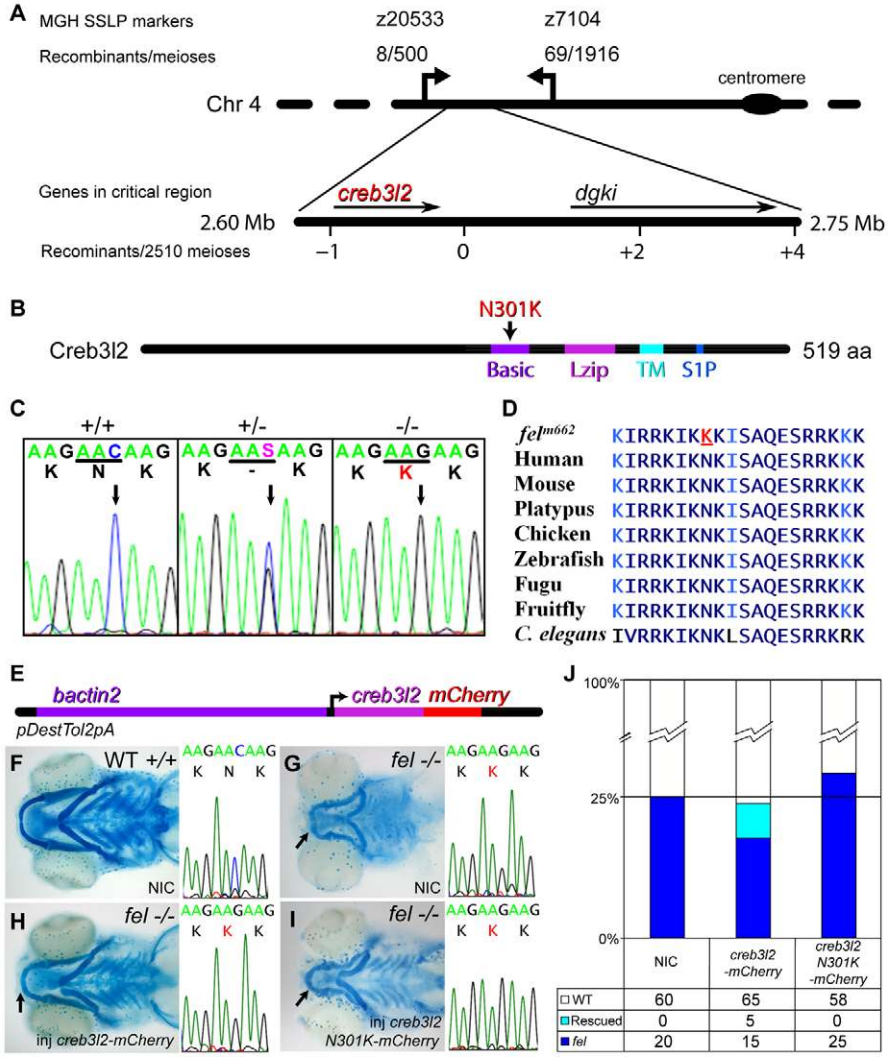

Fig. 5. The *feelgood* line carries a missense mutation in *creb3l2*. (A) The *feelgood* mutation was mapped to chromosome 4 between SSLP markers z20533 and z7104. Novel SSLP markers with the indicated number of recombinants reduced the critical interval to a ~50 kb region that contained two genes. The physical map of the critical region was based on the Zv7 assembly. (B) Schematic diagram of the Creb3l2 primary structure illustrating a missense N301K mutation in the DNA-binding basic motif. Basic, basic motif; Lzip, leucine zipper motif; TM, transmembrane domain; S1P, Site-1 protease recognition sequence. (C) Electropherograms of wild-type (+/+), heterozygous (+/–) and *feelgood* (–/–) genomic DNA. The arrow points to the C→G transversion that results in lysine for asparagine substitution at position 301 (N301K). (D) Comparison of the DNA-binding basic motif of *creb3l2* across several species. The amino acid changed in *feelgood* mutants is underlined in red. (E) Schematic diagram of the Tol2kit-based construct containing *mCherry*-tagged *creb3l2* under the ubiquitous *β-actin* (*bactin2*) promoter. (F-I) Alcian blue staining of cartilage elements at 5 dpf of non-injected (NIC) wild-type embryo (F); non-injected *feelgood* embryo (G); *creb3l2-mCherry* rescued *feelgood* mutant embryo (H); and mutant embryo injected with *feelgood* (N301K) *creb3l2-Cherry* that failed to rescue the phenotype (I). The chromatograms of sequences surrounding the *feelgood* lesion for the embryos shown in F-I have been included in the corresponding adjacent images. Arrows indicate an increased length of lower jaw in rescued mutant (H) compared with NIC *feelgood* control (G) or embryos injected with *creb3l2 N301K* (I). (J) Quantification of the number of mutant, wild-type and rescued phenotypes in the *β-actin2 creb3l2-mCherry* injection experiments. The *feelgood* genotype of these fish was confirmed by sequencing.

severe than the ones in *feelgood* mutants (Fig. 6B-D). Decreasing the amount of morpholino resulted in a milder phenotype more similar to *feelgood* (Fig. 6C,C′, quantified in Fig. 6F). To determine the specificity of the MO-2 phenotype, we co-injected morphants with mRNA of correctly spliced *creb3l2* and observed a suppression of the MO-2 phenotype in live larvae and Alcian blue skeletal preparations (Fig. 6E). Because the depletion of zygotic *creb3l2* transcript results in more severe defects than the ones in *feelgood*, it is likely that the *feelgood* mutation represents a hypomorphic allele with partial loss of Creb3l2 function.

The *feelgood* mutation reduces the transcriptional activity of Creb3l2

The *feelgood* variant results in a change of a single amino acid residue (N301K) within the DNA binding domain of Creb3l2. To assess whether this change affects transcriptional activity, we cloned zebrafish cDNAs encoding wild-type Creb3l2, the N-terminal 374 aa of Creb3l2 (which is similar to the S1P cleaved form of Creb3l2), and the corresponding *feelgood* variants into expression vectors (Fig. 7A). We also cloned the 895 bp fragment of the zebrafish *sec23a* promoter, which is located immediately upstream from the translation start site, in front of the *Luciferase* reporter gene. We chose this fragment because it contains three putative CREB-binding elements: 5′-TGACGTGG-3′ at position –3 to –10; 5′-TCACGTTT-3′ at –347 to –354 and 5′-AGACGTCT-3′ at –888 to –895 bp from the transcriptional start site.

Transient transfection experiments in human fibroblasts showed that the wild-type Creb3l2 and the processed, cytosolic Creb3l2 activate the reporter gene by 5.5- and 7.5-fold, respectively (Fig. 7B). By contrast, both the full-length and cytosolic *feelgood* Creb3l2 variants were considerably less active, inducing the promoter by 2.5- and 4.0-fold, respectively. The transcriptional activity assays suggest that the N301K *feelgood* variant diminishes the transcriptional activity of Creb3l2 by approximately 50%. Thus, the molecular data are consistent with the genetic and MO-mediated mutational analyses described above (Figs 5, 6), which show that *feelgood* is a hypomorphic allele. The fact that both the full-length and the processed Creb3l2 mutants display a similar loss of activity compared with the corresponding wild-type proteins strongly suggests that the primary molecular defect in *feelgood* leads to loss of transcriptional activity, or nuclear transport rates, rather than

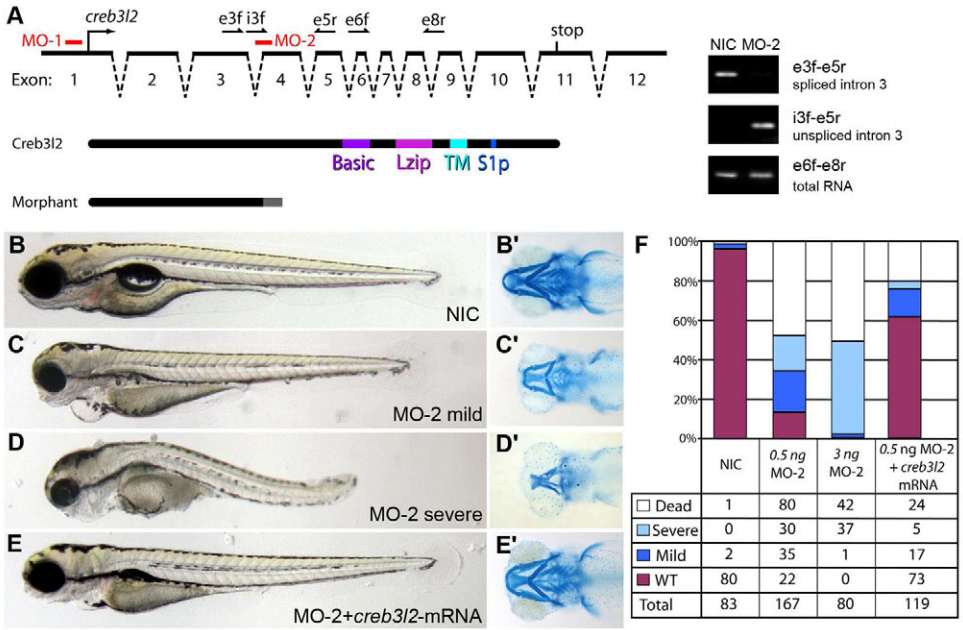

	NIC	0.5 ng MO-2	3 ng MO-2	0.5 ng MO-2 + creb3l2 mRNA
Dead	1	80	42	24
Severe	0	30	37	5
Mild	2	35	1	17
WT	80	22	0	73
Total	83	167	80	119

Fig. 6. Decreased Creb3l2 function is responsible for the *feelgood* phenotype. (A) Schematic representation of the *creb3l2* gene structure and positions of the two morpholinos MO-1 and MO-2 used in knockdown experiments. The names, position and orientation of specific primers used to evaluate the effectiveness of MO-2 are shown on top of the genomic locus diagram. Exonic primers are indicated by an 'e', intronic primers are indicated by an 'i'. The predicted truncated form of the protein caused by MO-2 compared with the full-length wild-type protein is shown below (Morphant). PCR amplification products representing spliced and unspliced *creb3l2* mRNA as compared with total *creb3l2* mRNA in embryos injected with 3 ng MO-2 is shown on the right gel electrophoresis images. The primers used for amplification are shown on the right images. (B-E′) Live (lateral; B-E) and Alcian blue stained (ventral; B′-E′) images of 80-hpf embryos injected with 0.5 ng MO-2 (C,D), or MO-2 plus *creb3l2*-mRNA (E). NIC, non-injected control is shown in B. (F) Quantification of knockdown and mRNA rescue experiments indicates the percentage of embryos in the four phenotypic classes observed.

incorrect processing by S1P or inefficient transport of Creb3l2 from ER to Golgi.

The *feelgood* mutation leads to decreased expression levels of select cargo adaptor proteins

Collectively, our results indicate that *feelgood* (*creb3l2*) mutants have a similar, although milder, craniofacial phenotype to *crusher* (*sec23a*) and *bulldog* (*sec24d*) mutants (Lang et al., 2006; Sarmah et al., 2010). This raises the possibility that the *feelgood* deficit leads to lower expression levels of *sec23a* and *sec24d.* Sec23A was previously shown to be a direct target of Creb3l2 (Saito et al., 2009). We also found that Creb3l2 itself has a conserved *cre* site in its promoter, and therefore might be self-regulated.

In order to determine whether the putative targets of Creb3l2 – *creb3l2*, *sec23a* and *sec24d* – are misregulated in *feelgood* mutants, we analyzed total RNA samples from 80-hpf embryos. We also included *sec24c* and *sec23b* for comparison. Quantitative real-time PCR (qPCR) results show that the expression levels of *creb3l2*, *sec23a* and *sec24d* are decreased in *feelgood* mutants relative to wild types (Fig. 7C). By contrast, *sec24c* levels are upregulated in *feelgood* mutants as compared with wild types. This outcome could be either due to *sec24c* upregulation through Creb3l2-independent, compensatory mechanisms, or a Creb3l2-mediated, indirect suppression of *sec24c*.

To determine whether expression levels of Creb3l2 targets are altered by disruption of ER-to-Golgi protein trafficking independently of Creb3l2, we analyzed RNA samples from *crusher* and *bulldog* mutants. The results show that the expression levels of *creb3l2*, *sec23a* and *sec24d* are increased in these mutants relative to wild types, except for *sec23a* and *sec24d* in their respective mutants, which might be due to nonsense-mediated decay (Fig. 7C), whereas *sec24c* is increased in all three mutants.

Taken together, these results demonstrate that Creb3l2 plays an important role in regulating multiple components of COPII carriers, as well as regulating its own expression. Interestingly, there is no evidence that the expression of *sec24c* is regulated by Creb3l2, consistent with the lack of craniofacial dysmorphology phenotype in *sec24c* morphants (Sarmah et al., 2010).

The *feelgood* mutation does not cause ER stress response

To test whether the unfolded protein response (UPR) is disrupted in *feelgood* mutants, we analyzed the expression of *bip* and *sil1* (Fig. 7D), both of which are induced in *crusher* and *bulldog*. Neither was upregulated in a statistically significant manner in 80-hpf *feelgood* mutants compared with wild types, suggesting a lack of ER stress response. Finally, expression differences in the Creb3l2 processing enzyme S1P were negligible in the three mutants. The lack of UPR probably reflects the less severe nature of the *feelgood* phenotype, consistent with the hypothesis that the primary *feelgood* defect is in collagen trafficking.

DISCUSSION

Here we show that the zebrafish *feelgood* mutation manifests skeletal phenotypes resembling those observed in *crusher* (*sec23a*)

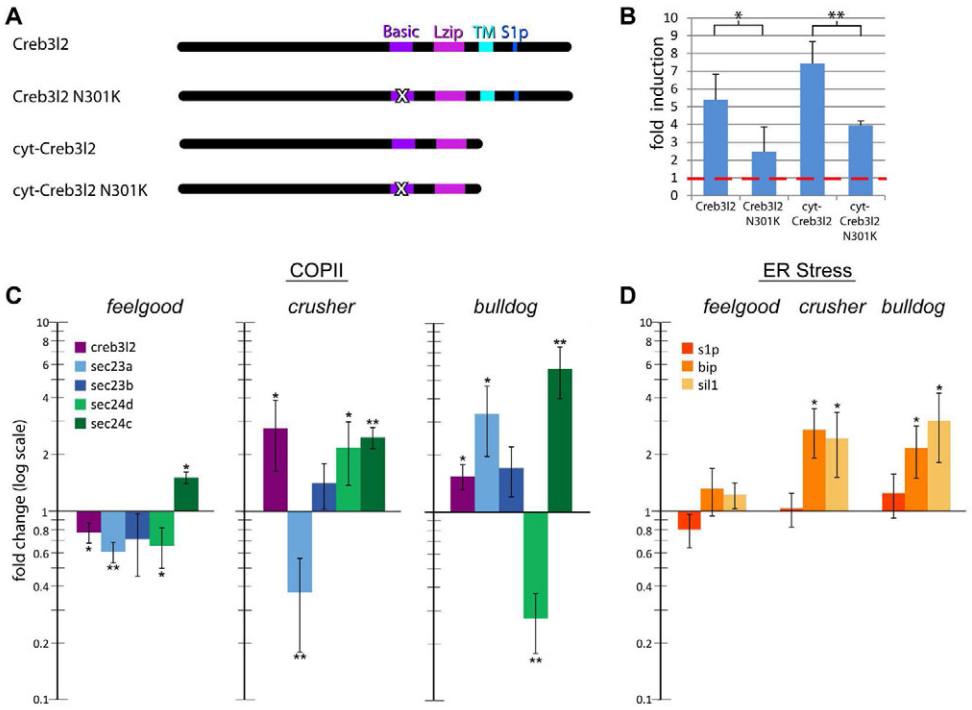

Fig. 7. Expression of gene transcripts encoding COPII components is reduced in *feelgood*. (A) Schematic of zebrafish Creb3l2 expression constructs. 'X' in the basic domain marks the *feelgood* N301K mutation. (B) Luciferase reporter assays. Human fibroblasts were transfected with the indicated expression constructs and the firefly luciferase reporter containing 0.8 kb of the zebrafish *sec23a* promoter. *Renilla* luciferase control plasmid was also used as transfection efficiency control. Luciferase activities were compared with those of cells transfected with empty vector to determine fold induction. Red line indicates baseline activity adjusted to *Renilla* luciferase values. (C,D) qPCR analysis of the fold expression change of COPII-related transcripts *creb3l2*, *sec23a*, *sec23b*, *sec24d* and *sec24c* (C), and ER-stress-related transcripts *s1p*, *bip* and *sil1* (D) in *feelgood*, *crusher* (*sec23a*) and *bulldog* (*sec24d*) mutants compared with wild types. RNA was extracted form whole embryos at 80 hpf. All results are normalized to β-actin and then to wild type. **P*<0.05; ***P*<0.005.

and *bulldog* (*sec24d*), i.e. accumulation of type II and type IV collagens within enlarged rough ER in chondrocytes and notochord sheath cells. At the molecular level, the *feelgood* mutation causes an amino acid substitution within the DNA-binding domain of the transcription factor Creb3l2.

feelgood mutants present deficits in the late developmental stages of the craniofacial skeleton formation. The early stages of head skeleton development, including neural crest migration, mesenchymal condensation and specification into type II collagen secreting chondrocytes, proceed normally, indicating that these steps do not depend on fully functional Creb3l2. However, in the later developmental steps, characterized by robust collagen secretion by chondrocytes, ECM fails to densify and mature, leading to skeletal elements that are specified, but structurally malformed. This phenotype of normal skeletal patterning and misshapen individual elements is similar to human birth defects including CLSD (Boyadjiev et al., 2006; Fromme et al., 2007), and, as such, *feelgood* might provide a powerful tool for understanding the etiology of this class of congenital dysmorphologies. Moreover, the initial presence of collagen fibrils in the extracellular space, but lack of ECM maintenance seen in *feelgood* mutants, is reminiscent of adult-onset diseases characterized by microarchitectural skeletal deterioration such as observed in osteoporosis or arthritis (Goldring and Goldring, 2010; Heinegård and Saxne, 2011).

Our results uncovered that Creb3l2 function is not confined to skeletal tissues, but is also required in other cell types. Specifically, *feelgood* mutant embryos displayed defects in the maturation of melanosomes; these defects are similar to those previously described in the zebrafish and mouse mutation *silver* (Schonthaler et al., 2005; Theos et al., 2006). The *silver* locus encodes Pmel17, a type I membrane-inserted glycoprotein that is an integral part of the melanosomal matrix. Pmel17 is trafficked from the ER to endosomes and finally to melanosomes (Theos et al., 2005; Harper et al., 2008). In *feelgood*, as revealed by TEM, the trafficking of melanosome matrix proteins that are responsible for change in melanosome shape is de-coupled from pigment synthesis and secretion, indicating that Creb3l2-mediated regulation of cargo secretion extends to different cell types.

Creb3l2 is a protein of 519 amino acids, coded by 12 exons spanning a genomic region of over 120 kb. The overall genomic structure as well as the amino acid sequence of the DNA-binding domain have been highly conserved from zebrafish to human (Storlazzi et al., 2003). Creb3l2 is part of a class I membrane-bound basic leucine zipper proteins that must be cleaved by S1P and Site-2 protease (S2P) in order to be activated (Fig. 8) (Seidah et al., 1999; Kondo et al., 2007). Because Creb3l2 is synthesized in the ER, whereas the proteases that cleave it are localized in the Golgi, Creb3l2 proteolysis might be regulated by the availability of the COPII machinery as with the similarly cleaved sterol regulatory element binding proteins (SREBPs) (Espenshade et al., 2002). Thus, by virtue of being an ER-resident protein, Creb3l2 is in an ideal location to optimize both the availability and composition of the ER-to-Golgi trafficking machinery by selective regulation of secretory pathway components.

Previously, Creb3l2 was shown to directly bind the promoter of *Sec23a* in mouse (Saito et al., 2009). Our analysis using the zebrafish *sec23a* promoter and constructs encoding wild-type and mutant Creb3l2 show that Creb3l2 N301K has lost approximately 50% of its transcriptional activity. This result further corroborated the mild skeletal defects observed in *feelgood* mutants. Thus, we concluded that the *feelgood* mutation represents a hypomorphic allele that is much less severe than the zebrafish *creb3l2* morphants and knockout mouse, both of which have very severe skeletal deficits.

The analysis of Creb3l2 KO mice has suggested that the Creb3l2-mediated Sec23a pathway regulates the ER stress response

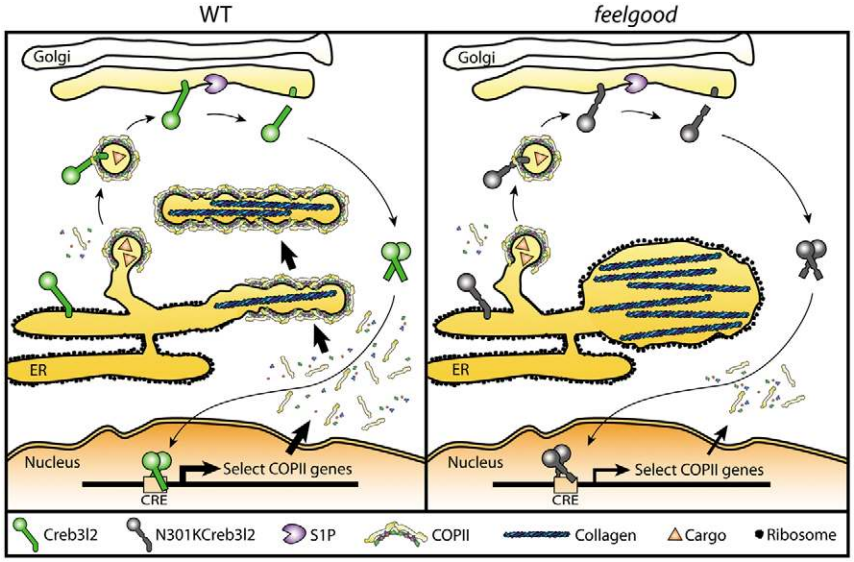

Fig. 8. Model of Creb3l2 function and the phenotype of the *feelgood* mutation. When the secretory load of a wild-type cell (left panel) increases beyond the capacity of the basal level of COPII protein expression, Creb3l2, which is normally localized in the ER, is cleaved by cis-Golgi-resident S1P. After cleavage, Creb3l2 dimerizes and enters the nucleus to bind *cre* sites in the promoters of select COPII genes, upregulating their expression and increasing the secretory capacity of cell. In *feelgood* mutants (right panel), the missense mutation in the DNA-binding domain of Creb3l2 probably leaves the regulatory steps of cleavage and dimerization unaffected, but leads to inefficient binding of Creb3l2 to *cre* sites and diminished upregulation of expression of COPII components. The lack of adequate secretory machinery leads to distended ER filled with collagen, whereas trafficking of small cargos such as glycosaminoglycans and some large cargos such as laminin is unaffected. This might be due to insufficient levels of COPII components to build the more complex structures required for large cargos, or large cargos might be displaced by smaller ones when the secretory capacity is limited, or because Creb3l2 differentially regulates COPII paralogs Sec24C and Sec24D, leading to deficient Sec24-dependent cargo sorting caused by an improper balance of Sec24 proteins.

machinery during chondrogenesis (Saito et al., 2009). We detected similar increases in the ER stress response in *crusher* (*sec23a*) and *bulldog* (*sec24d*) mutants, but not in *feelgood*. It has been difficult to discern which aspects of the phenotype are due to overactivation of the ER stress response and which are due to the inability of cells to secrete proteins to build normal ECM. However, the hypomorphic nature of the *feelgood* allele allowed us to parse the ER stress response phenotype from the requirement of Creb3l2 for COPII-dependent ER-to-Golgi transport. We postulate that the primary function of Creb3l2 is not direct regulation of the ER stress response. This conclusion is consistent with our preliminary results using additional ER stress response markers, such as CHOP and Xbp1 (Tabas and Ron, 2011) (data not shown). These experiments did not reveal significant upregulation of ER stress response in *feelgood* mutants or in the much more severe *creb3l2* morphants.

We have shown that Creb3l2 does not only regulate the expression of *sec23a*, but also that of other COPII components, namely *sec23b* and *sec24d*. Although we observed diminished expression of *sec24d* in *feelgood*, we did not find any evidence that Creb3l2 regulates the expression of the closest paralog of *sec24d*, *sec24c*. Therefore, it is likely that the *feelgood* mutation mostly affects the Creb3l2-Sec24D secretory axis without influencing Sec24C-dependent cargos. The loss-of-function phenotypes of *creb3l2*, *sec24d* and *sec24c* mutants and/or morphants support this model (Sarmah et al., 2010; Melville and Knapik, 2011). For example, the four *bulldog* zebrafish alleles, which abolish Sec24D function, share many features with *feelgood*, i.e. they display intracellular backlogs of collagen molecules and sparse ECM but relatively normal trafficking of other ECM molecules such as fibronectin (Sarmah et al., 2010). By contrast, chondrocyte maturation and skeletal development proceed normally in *sec24c* morphants.

The differential transcriptional regulation of COPII components could also explain the tissue-specific deficits observed in some human syndromes. For example, mutations in SEC23B result in the human disease CDAII, which manifests in anemia but not skeletal defects, whereas mutations in SEC23A result in the human disease CLSD, which is characterized by skeletal defects but not anemia (Boyadjiev et al., 2006; Bianchi et al., 2009). The differences in phenotypes might be due to divergent transcriptional regulation, resulting in differential availability of various COPII components in different cell types. This hypothesis is supported by the finding that SEC23B is expressed at fivefold higher levels than SEC23A in human erythroblasts (Schwarz et al., 2009). Because both Sec23 paralogs are *Creb3l2* targets, it is likely that additional unknown regulators modulate the availability of Sec23A, Sec23B, Sec24C and other COPII-associated proteins. Future discovery research in this area is likely to help crack the secretory code.

The high ECM secretory load has been postulated as a cause of the craniofacial dysmorphology in the COPII mutants (Lang et al., 2006; Fromme et al., 2007). Our results suggest that Creb3l2 is also required for the secretion of certain protein classes independently of secretory volume. For example, Collagen II and IV secretion to the extracellular space is affected in both chondrocytes and notochord sheath cells, yet the latter produce far fewer collagen fibrils than the former. Moreover, although fibrillar collagens accumulate in intracellular compartments, other abundantly

deposited ECM proteins such as laminins, as well as vacuolar GAG proteins, are trafficked to the extracellular space.

There are several explanations of how this phenotype might occur. It is plausible that large fibrillar molecules such as collagen compete less efficiently with other protein classes that are synthesized in the ER and destined for transport to Golgi and subsequent destinations. This might occur because, whereas cargo-free self-assembled COPII vesicles are 40-80 nm in diameter (Barlowe et al., 1994; Miller and Barlowe, 2010; Dancourt and Barlowe, 2010), fibrillar procollagen bundles form rigid 300 nm rods (Fraser et al., 1979; Stephens and Pepperkok, 2002; Canty and Kadler, 2005). Hence, collagen transport requires specialized, oversized COPII structures and an ample supply of coat proteins (Stagg et al., 2008; O'Donnell et al., 2010). As a result, in cells with high levels of protein trafficking, the availability of COPII carriers might become a limiting factor, and other proteins might displace collagen molecules. Alternatively, there might be insufficient levels of COPII components to build the more complex tubular structures required for large cargos, leading to intracellular backlogs of collagen within distended ER compartments (Fig. 8, right).

Craniofacial and skeletal dysmorphologies account for the majority of birth defects and most of them are of unknown origin. The fact that random mutagenesis screens in zebrafish have yielded multiple mutants that disrupt the transport machinery suggests that at least some of the birth defects of unknown nature are due to abnormal protein transport (Neuhauss et al., 1996). Besides developmental defects, a host of adult-onset human diseases, including arthritis or interstitial fibrosis after organ injury, have been linked to dysregulated collagen production (Goldring and Marcu, 2009; Goldring and Goldring, 2007; Heinegård and Saxne, 2011; Trojanowska et al., 1998). The decoupling of collagen transport from that of other cargos as well as the hypomorphic nature of the *feelgood* allele has important implications in the understanding of human diseases linked to collagen defects. Because the genetic basis for these diseases is often highly complex, tools such as *feelgood* are important for identifying potential candidate genes and regulatory networks. Better understanding of the roles of the regulatory and structural components of the intracellular transport machinery could lead to better diagnostic tools and novel treatments of human diseases.

METHODS

Fish maintenance and breeding

Fish were raised and kept under standard laboratory conditions at 28.5°C as previously described (Barrallo-Gimeno et al., 2004; Montero-Balaguer et al., 2006). *feelgood* [allele designated *m662*, isolated in the MGH genetic screen (Neuhauss et al., 1996; Driever et al., 1996)] was kept in AB genetic background for phenotypic analysis. Embryos were staged and fixed at specific hours (hpf) or days (dpf) post-fertilization as described by Kimmel et al. (Kimmel et al., 1995). For some experiments embryos were incubated in 0.2 mM 1-phenyl-2-thiourea (Sigma) to block pigmentation.

Genetic mapping and cloning

The *feelgood* locus was mapped in an F2 intercross using bulked segregate analysis. DNA samples were PCR-genotyped with SSLP markers evenly spaced across the zebrafish genome. The mapped *feelgood* mutation was confirmed by sequencing genomic DNA flanking the mutation site from three homozygous wild-type F2 animals, five heterozygous F2 animals, six homozygous mutant F2 animals and six animals each from three different genetic backgrounds of wild-type fish (AB, IN and TL).

Cartilage staining

Embryos (80 hpf or 5 dpf) were fixed in 4% phosphate buffered PFA overnight. After two washes in PBS (1×) for 5 minutes, embryos were bleached with 10% H_2O_2 and 30 µl of 1 M KOH for 1 hour. Following two washes in PBT for 5 minutes, embryos were incubated in 0.1% Alcian blue solution overnight at room temperature (RT) on a shaker. After one wash in acidic ethanol (70% ethanol, 5% HCl) followed by an overnight destaining in fresh acidic ethanol, embryos were dehydrated in 85% and 100% ethanol for 15 minutes each and transferred to 80% glycerol.

Histology

Histological sections were prepared in JB-4 plastic resin medium (Polysciences). Phosphate buffered PFA (4%)-fixed 5-dpf embryos were washed with PBS and subsequently dehydrated with 25%, 50%, 70% and 95% ethanol (each step for 5 minutes). Dehydrated embryos were equilibrated with JB-4 infiltration solution for 10 minutes at RT. The embryos were then placed in plastic molds and mounted in JB-4 embedding solution. Blocks were sectioned in 5 µm thickness using a Leica RM2265 microtome. Sections were collected on adhesive coated slides (Superfrost plus, Fisher), dried on a heating plate and stained with metachromatic dye Toluidine blue (Sigma), and mounted using cytoseal-XYL as a mounting medium as previously described (Granero-Moltó et al., 2008).

Immunofluorescence and WGA staining

Type II collagen and WGA staining was performed as previously described (Sarmah et al., 2010). Whole-mount embryos were fixed in 4% PFA at 4°C overnight and incubated with 1:200 diluted primary antibody against collagen type II (Polysciences) and WGA–Alexa-Fluor-488 conjugate (1:200) followed by 1:300 Alexa Fluor 555 fluorescently conjugated secondary antibody (Molecular Probes). The WGA lectin binds to N-acetylglucosamine and N-acetylneuraminic acid residues of membrane and matrix glycoproteins. For staining on sections, embryos were fixed in 4% or 2% PFA, embedded in 1.5% agarose in 5% sucrose, and stored in 30% sucrose solution at 4°C overnight. Agarose blocks were mounted with O.C.T. (Sakura Finetechnical). 15-µm sections were cut using a Leica CM 3050 cryostat at –20°C and transferred onto Superfrost slides (Fisher). Sections were washed in PBS, blocked in 2 mg/ml BSA, 2% goat serum, 2% DMSO in PBS and incubated with collagen type II antibody (1:250 dilution), collagen type IV antibody (1:200 dilution, Lab Vision), Laminin Ab-1 (1:100; LabVision) or WGA (1:250) at 4°C overnight. Alexa-Fluor-555 or Alexa-Fluor-488 conjugate was applied as secondary antibody (1:500). TO-PRO-3 (Molecular Probes) was used for nuclear counterstaining. Confocal images were taken with a Zeiss LSM510 inverted confocal microscope (Vanderbilt Cell Imaging Shared Resource).

Electron microscopy

After being anesthetized with tricaine (Sigma), zebrafish embryos were placed into fresh 2% gluteraldehyde and incubated overnight

at 4°C. Fish were washed in PBS, transferred to 1% osmium textroxide and washed in diH_2O. Fish were stained en bloc in 1% aqueous uranyl acetate for 1 hour and washed in diH_2O. The samples were taken through a series of dehydration steps starting with 30% and followed by 50%, 70%, 95% and absolute ethanol. Propylene oxide was used as a transitional solvent to replace the dehydration solution. Samples were transferred to a 1:1 araldite:propylene oxide mixture then placed in pure araldite in a vacuum oven. Pure resin specimens were then transferred into embedding molds containing fresh resin and finally placed into a 16°C oven overnight. Ultra-thin serial sections (50-60 nm) from polymerized blocks were obtained using a Leica UCT Ultracut microtome (Leica Microsystems), transferred to Formvar-coated slot grids and examined using a Phillips CM10 TEM (FEI Company, Hillsboro, OR) equipped with an Advantage Plus 2 mega pixel Digital CCD System for CM10 TEM (Advanced Microscopy Techniques, Danvers, MA).

Western blotting

Proteins were isolated by homogenizing 4-dpf embryos in RIPA buffer containing protease inhibitor (Sigma). Glycoproteins in lysate were cleaved by Endo H (NEB) or PNGase F (NEB) according to manufacturer specifications. Proteins were separated by sodium dodecyl sulfate-polyacrylamide gel electrophoresis (SDS-PAGE) on 10% Mini-Protean TGX gels (Bio-Rad). For immunoblotting, proteins were transferred to polyvinylidene fluoride (PVDF) membrane using an electrophoretic transfer apparatus (Bio-Rad). The membrane was blocked with 1% non-fat milk (Bio-Rad) and incubated with 1:1000 diluted primary antibody against type II collagen (Polysciences), or N-Cadherin (Sigma) followed by 1:10,000 HRP-conjugated anti-rabbit secondary antibodies (Promega). Signal detection was performed using Pico West Chemiluminescent Substrate (Thermo Scientific).

Generation of Tol2kit-based transgenic fish

The *bactin2:creb3l2:mcherry* construct was created using the 'Tol2kit' approach (Kwan et al., 2007). In brief, PCR was used to add attB1 and attB2 sites to the coding region of *creb3l2*, and the product was recombined into pDONR221 to create a middle entry clone. A construct containing the N301K mutation was created using the QuikChange site-directed mutagenesis kit (Stratagene).

The final constructs were created by recombining the middle entry clone with p5E-bactin2, p3E-mCherrypA and pDestTol2pA2 as described in the Invitrogen Multisite Gateway manual. PCR products were purified using the Qiaquick gel extraction kit (Qiagen).

5′-capped sense RNAs were synthesized using a construct encoding the transposase and the mMessage mMachine kit (Ambion). 30 pg of the *bactin2:creb3l2-mCherry* construct and 20 pg of the transposase sRNA were simultaneously injected into embryos at the one-cell stage.

Phylogenetic analysis

Protein sequences were aligned using ClustalW2 (http://www.ebi.ac.uk/Tools/clustalw2/index.html). A phylogenetic tree was constructed using the neighbor joining method (Saitou and Nei, 1987).

RNA isolation and RT-PCR analysis

RNA was extracted and reverse transcription performed as described (Müller et al., 2006). cDNA was used as template for PCR analysis of *creb3l2* expression between the one-cell stage and 5 dpf. The exon-spanning primers amplified a 235 bp fragment and were as follows: βactin 5′-GACTCAGGATGCGGAAACTG-3′, 5′-AAGTCCTGCAAGATCTTCAC-3′; Creb3l2 5′-CACAGAAC-CACCACCATGAG-3′, 5′-ACAGGAGAGTCGCAGGAAAA-3′.

Morpholino knockdown

Antisense morpholino oligonucleotides (MOs) (Gene Tools) were designed to target the *creb3l2* 5′UTR (MO-1: 5′-CAGCGTCGCTTCAACGACCCCAGAA-3′), or the *creb3l2* intron3-exon4 boundary (MO-2: 5′-CAGACCTGGA-CAACAGCATGACACT-3′). MO concentrations were determined spectrophotometrically and 1 nl was injected into one- to two-cell stage embryos at increasing doses (0.25-8 ng) to determine optimal concentrations. MO-1 was injected at 7 ng, and MO-2 was injected at 0.5 ng and 3 ng (Fig. 6B-F, live images and Alcian blue stains are of embryos injected at 0.5 ng). Both morpholinos produced similar phenotypes, and MO-2 was used for all experiments pictured. MO-2 effectiveness was evaluated at 3 ng using primers indicated in Fig. 6A, with sequences: e3f 5′-CTTGAACCTCTCGCCTAAAG-3′, i3f 5′-GCCATGATTGAGCGTTCAGT-3′, e5r 5′-ATCCTTC-AGCAATGAGGGTC-3′, e6f 5′-ACAGGAGAGTCGCA-GGAAAA-3′ and e8r 5′-CACAGAACCACCACCATGAG-3′.

In situ hybridization

The *creb3l2* probe was made by cloning 427 nucleotides from the 3′UTR of *creb3l2* cDNA into pGEM-T Easy vector (Promega) with primers 5′-ATCTACTGCGCTGGGGCGAT-3′ and 5′-AATA-TTTTCCTTAATAAAAGCA-3′. Whole-mount in situ hybridization was performed as previously described (Sachdev et al., 2001).

Pigment aggregation assay

3-dpf embryos were placed in egg water containing 0.5 μg/ml 4-hydroxyanisole (Sigma) for 3 days and imaged. 6-dpf embryos were placed in egg water containing 1 nM melanin concentrating hormone (Sigma) for 10 minutes (Logan et al., 2006).

Luciferase assay

Effector protein expression plasmids were generated by subcloning full-length and cytosolic-domain (1-374) Creb3l2 and N301KCreb3l2 into pCS2+ vector. The firefly luciferase reporter plasmid was generated by subcloning 895 bp of promoter sequence upstream of zebrafish *sec23a* into the pGL3 luciferase reporter vector (Promega). Human foreskin fibroblasts (System Biosciences) were grown to 95% confluency and transfected using Lipofectamine 2000 (Invitrogen) according to the manufacturer's specifications with reporter plasmid (0.4 μg), the corresponding effector plasmids (0.4 μg), and a reference plasmid pRL-SV40 (0.04 μg) carrying the *Renilla luciferase* gene under the control of the SV40 enhancer and promoter (Promega). After 30 hours, luciferase activities were measured using the Dual-Luciferase Reporter Assay System (Promega) according to the manufacturer's protocol. Firefly luciferase activity was normalized to that of *Renilla* luciferase.

TRANSLATIONAL IMPACT

Clinical issue

Normal cellular function depends on an elaborate network of intracellular organelles and molecular carriers that direct traffic of individual proteins to specific destinations. The journey of membrane-embedded or secreted proteins such as cell adhesion molecules, growth factors and extracellular matrix (ECM) begins in the endoplasmic reticulum (ER). Proteins synthesized in the ER are subsequently transported to the Golgi complex, where they become glycosylated before being sent to other organelles, the cell surface or the extracellular space. Transport from the ER to the Golgi is conducted by the coat protein II (COPII) vesicular carriers, which take part in various enzymatic activities, cargo recognition and structural assembly.

Over the last few years it has become evident that genetic defects in genes encoding COPII components cause developmental abnormalities in embryos, as well as a wide range of human diseases in adults, from anemia to skeletal deformities and lipid malabsorption. Besides genetic defects, interstitial fibrosis leading to organ failure after injury, or pathological conditions in aging patients such as arthritis, have been associated with dysregulated, often excessive, protein secretion.

Results

The authors show that the *feelgood* mutation in zebrafish is caused by a single amino acid substitution within the DNA-binding domain of transcription factor Creb3l2, which is known to be a positive regulator of secretory pathway proteins. Although this mutation has a relatively moderate impact on Creb3l2 activity, it causes severe skeletal defects. Using histological and molecular approaches, the authors demonstrate that the primary deficit is the abnormal accumulation of collagen molecules, which fail to be exported from the ER of chondrocytes and notochord cells. The authors also present evidence that the function of Creb3l2 is not confined to skeletal tissues, but extends to other cell types, including organelle assembly in melanocytes.

Surprisingly, other abundantly deposited ECM proteins such as laminin are trafficked in a normal fashion, suggesting that Creb3l2 is required for the transport of specific protein classes. This might be because Creb3l2 regulates expression of only a select subset of genes that encode transport machinery units. Thus, Creb3l2 seems to be a key regulator of both the availability and composition of COPII vesicular carriers, which could explain how different cell types secrete specific proteins.

Implications and future directions

The findings presented here imply that skeletal morphogenesis is particularly sensitive to both the precise levels and molecular composition of the transport machinery. A large number of identified craniofacial mutations in animal models disrupt protein trafficking with high frequency, strongly suggesting that at least some of the birth defects of unknown origin are due to abnormal protein transport. Future analyses will focus on genetic screens and genomic approaches to search for human variants in key regulatory and structural modules of protein secretion, as well as on studies aiming to further understand the molecular mechanisms behind the variable transport rates of specific protein classes in different cell types. This knowledge might improve future diagnosis and management of a broad spectrum of human diseases.

Quantitative PCR analysis

qPCR was performed as described previously (Sarmah et al., 2010). Total RNA was extracted from approximately 30 embryos at different embryonic time points using the TRIzol reagent (Sigma). 2 mg of total RNA were reverse transcribed to cDNA using M-MLV reverse transcriptase (Promega) and poly-T primer. Each PCR reaction was performed with 1 µl of cDNA using iQ SYBR Green Supermix (Bio-Rad) and 5 µM of each primer. Primer sets used were: βactin: 5′-GACTCAGGATGCGGAAACTG-3′, 5′-AAGTCCTGCAAGATCTTCAC-3′, Creb3l2: 5′-ACAGGAGAGTCGCAGGAAAA-3′, 5′-CACAGAACCACCACCATGAG-3′, Sec23a: 5′-AGGTGGACGTGGAGCAATAC-3′, 5′-CGAGAACGTCTCGGAGAAAC-3′, Sec23b: 5′-ATGCTGGGACTGATGAAACC-3′, 5′-TCCTGTGTTTGGGAAAGTCC-3′, Sec24D: 5′-TTTGCTGACACCAACGAGAG-3′, 5′-TGATTGGGGAACAGGAAGAG-3′, Sec24c: 5′-CAGGGAAGAGAGTGGACTGC-3′, 5′-GTCTTCAGCTCCTGGCAAAC-3′, S1P: 5′-GGATGTGGCGGTGTCTTACT-3′, 5′-CCTCTTACTGCGTGGAGGAG-3′, Bip: 5′-CAGGAAAGAGTAAAACAGCAACCG-3′, 5′-CCGAAATTTTGCTCTCACTGCATC-3′, and Sil1: 5′-CAGGAAAGAGTAAAACAGCAACCG-3′, 5′-CCGAAATTTTGCTCTCACTGCATC-3′.

Three independent experiments in triplicates were performed using β-actin as internal control. Thermal cycling was carried out in an iQ5 (Bio-Rad) and relative expressions were calculated following previously described methods (Livak and Schmittgen, 2001).

Statistical analysis

Data in bars represent average ± s.d. Statistical analyses were performed using unpaired two-tailed Student's *t*-test and *P*-values <0.05 were considered as significant.

ACKNOWLEDGEMENTS

We thank Cory Guthrie and Witold Rybski for excellent animal care, Kirill Zavalin for help with experiments, and Wolfgang Driever for sharing the *feelgood* mutant and wild-type zebrafish lines. We are indebted to Anne Kenworthy and Jason Jessen for critically reading the manuscript. The work has been supported by the NIH NIDCR grant R01 DE018477 (E.W.K.), NHLBI HL083958 and HL100398 (A.K.H.), NIDDK DK65637 (J.R.S.), NIGMS T32 GM008554, the Cellular, Biochemical and Molecular Sciences Training Program at Vanderbilt (D.B.M.), and CHHD T32 HD007502-14 Vanderbilt University, Training Program in Developmental Biology (D.S.L.).

COMPETING INTERESTS

The authors declare that they do not have any competing or financial interests.

AUTHOR CONTRIBUTIONS

Conceived and designed the experiments: D.B.M., A.K.H., E.W.K. Performed the experiments: D.B.M., M.M.-B., D.S.L. Analyzed the data: D.B.M., A.K.H., E.W.K. Contributed reagents/materials/analysis tools: K.B., J.R.S. Wrote the paper: D.B.M., A.K.H., E.W.K. Corrected manuscript drafts: E.W.K., A.K.H., D.S.L., D.B.M.

SUPPLEMENTARY MATERIAL

Supplementary material for this article is available at http://dmm.biologists.org/lookup/suppl/doi:10.1242/dmm.007625/-/DC1

REFERENCES

Adams, D. S., Keller, R. and Koehl, M. A. (1990). The mechanics of notochord elongation, straightening and stiffening in the embryo of Xenopus laevis. *Development* **110**, 115-130.

Allen, R., Schroeder, C. and Fok, A. (1989). Intracellular binding of wheat germ agglutinin by Golgi complexes, phagosomes, and lysosomes of Paramecium multimicronucleatum. *J. Histochem. Cytochem.* **37**, 195-202.

Aridor, M. and Hannan, L. A. (2002). Traffic jams II: an update of diseases of intracellular transport. *Traffic* **3**, 781-790.

Barlowe, C., Orci, L., Yeung, T., Hosobuchi, M., Hamamoto, S., Salama, N., Rexach, M. F., Ravazzola, M., Amherdt, M. and Schekman, R. (1994). COPII: a membrane coat formed by Sec proteins that drive vesicle budding from the endoplasmic reticulum. *Cell* **77**, 895-907.

Barrallo-Gimeno, A., Holzschuh, J., Driever, W. and Knapik, E. W. (2004). Neural crest survival and differentiation in zebrafish depends on mont blanc/tfap2a gene function. *Development* **131**, 1463-1477.

Bianchi, P., Fermo, E., Vercellati, C., Boschetti, C., Barcellini, W., Iurlo, A., Marcello, A. P., Righetti, P. G. and Zanella, A. (2009). Congenital dyserythropoietic anemia type II (CDAII) is caused by mutations in the SEC23B gene. *Hum. Mutat.* **30**, 1292-1298.

Boyadjiev, S. A., Fromme, J. C., Ben, J., Chong, S. S., Nauta, C., Hur, D. J., Zhang, G., Hamamoto, S., Schekman, R., Ravazzola, M. et al. (2006). Cranio-lenticulo-sutural

dysplasia is caused by a SEC23A mutation leading to abnormal endoplasmic-reticulum-to-Golgi trafficking. *Nat. Genet.* **38**, 1192-1197.

Bradley, K., Elmore, J. B., Breyer, J., Yaspan, B., Jessen, J., Knapik, E. and Smith, J. (2007). A major zebrafish polymorphism resource for genetic mapping. *Genome Biol.* **8**, R55.

Canty, E. G. and Kadler, K. E. (2005). Procollagen trafficking, processing and fibrillogenesis. *J. Cell Sci.* **118**, 1341-1353.

Dancourt, J. and Barlowe, C. (2010). Protein sorting receptors in the early secretory pathway. *Annu. Rev. Biochem.* **79**, 777-802.

DeLise, A. M., Fischer, L. and Tuan, R. S. (2000). Cellular interactions and signaling in cartilage development. *Osteoarthr. Cartil.* **8**, 309-334.

Driever, W., Solnica-Krezel, L., Schier, A. F., Neuhauss, S. C., Malicki, J., Stemple, D. L., Stainier, D. Y., Zwartkruis, F., Abdelilah, S., Rangini, Z. et al. (1996). A genetic screen for mutations affecting embryogenesis in zebrafish. *Development* **123**, 37-46.

Espenshade, P. J., Li, W.-P. and Yabe, D. (2002). Sterols block binding of COPII proteins to SCAP, thereby controlling SCAP sorting in ER. *Proc. Natl. Acad. Sci. USA* **99**, 11694-11699.

Fraser, R. D., MacRae, T. P. and Suzuki, E. (1979). Chain conformation in the collagen molecule. *J. Mol. Biol.* **129**, 463-481.

Fromme, J. C., Ravazzola, M., Hamamoto, S., Al-Balwi, M., Eyaid, W., Boyadjiev, S. A., Cosson, P., Schekman, R. and Orci, L. (2007). The genetic basis of a craniofacial disease provides insight into COPII coat assembly. *Dev. Cell* **13**, 623-634.

Goldring, M. B. and Goldring, S. R. (2007). Osteoarthritis. *J. Cell. Physiol.* **213**, 626-634.

Goldring, M. B. and Marcu, K. B. (2009). Cartilage homeostasis in health and rheumatic diseases. *Arthritis Res. Ther.* **11**, 224.

Goldring, S. R. and Goldring, M. B. (2010). Bone and cartilage in osteoarthritis: is what's best for one good or bad for the other? *Arthritis Res. Ther.* **12**, 143.

Granero-Moltó, F., Sarmah, S., O'Rear, L., Spagnoli, A., Abrahamson, D., Saus, J., Hudson, B. G. and Knapik, E. W. (2008). Goodpasture antigen-binding protein and its spliced variant, ceramide transfer protein, have different functions in the modulation of apoptosis during zebrafish development. *J. Biol. Chem.* **283**, 20495-20504.

Harper, D. C., Theos, A. C., Herman, K. E., Tenza, D., Raposo, G. and Marks, M. S. (2008). Premelanosome amyloid-like fibrils are composed of only Golgi-processed forms of Pmel17 that have been proteolytically processed in endosomes. *J. Biol. Chem.* **283**, 2307-2322.

Heinegård, D. and Saxne, T. (2011). The role of the cartilage matrix in osteoarthritis. *Nat. Rev. Rheumatol.* **7**, 50-56.

Hickok, N. J., Haas, A. R. and Tuan, R. S. (1998). Regulation of chondrocyte differentiation and maturation. *Microsc. Res. Tech.* **43**, 174-190.

Hope, I. A. and Struhl, K. (1987). GCN4, a eukaryotic transcriptional activator protein, binds as a dimer to target DNA. *EMBO J.* **6**, 2781-2784.

Hynes, R. O. (2009). The extracellular matrix: not just pretty fibrils. *Science* **326**, 1216-1219.

Kimmel, C. B., Ballard, W. W., Kimmel, S. R., Ullmann, B. and Schilling, T. F. (1995). Stages of embryonic development of the zebrafish. *Dev. Dyn.* **203**, 253-310.

Knapik, E. W., Goodman, A., Ekker, M., Chevrette, M., Delgado, J., Neuhauss, S., Shimoda, N., Driever, W., Fishman, M. C. and Jacob, H. J. (1998). A microsatellite genetic linkage map for zebrafish (Danio rerio). *Nat. Genet.* **18**, 338-343.

Kondo, S., Saito, A., Hino, S., Murakami, T., Ogata, M., Kanemoto, S., Nara, S., Yamashita, A., Yoshinaga, K., Hara, H. et al. (2007). BBF2H7, a novel transmembrane bZIP transcription factor, is a new type of endoplasmic reticulum stress transducer. *Mol. Cell. Biol.* **27**, 1716-1729.

Kwan, K. M., Fujimoto, E., Grabher, C., Mangum, B. D., Hardy, M. E., Campbell, D. S., Parant, J. M., Yost, H. J., Kanki, J. P. and Chien, C.-B. (2007). The Tol2kit: a multisite gateway-based construction kit for Tol2 transposon transgenesis constructs. *Dev. Dyn.* **236**, 3088-3099.

Lang, M. R., Lapierre, L. A., Frotscher, M., Goldenring, J. R. and Knapik, E. W. (2006). Secretory COPII coat component Sec23a is essential for craniofacial chondrocyte maturation. *Nat. Genet.* **38**, 1198-1203.

Livak, K. J. and Schmittgen, T. D. (2001). Analysis of relative gene expression data using real-time quantitative PCR and the $2^{-\Delta\Delta C_T}$ method. *Methods* **25**, 402-408.

Logan, D. W., Burn, S. F. and Jackson, I. J. (2006). Regulation of pigmentation in zebrafish melanophores. *Pigment Cell Res.* **19**, 206-213.

Löppönen, T., Körkkö, J., Lundan, T., Seppänen, U., Ignatius, J. and Kääriäinen, H. (2004). Childhood-onset osteoarthritis, tall stature, and sensorineural hearing loss associated with Arg75-Cys mutation in procollagen type II gene (COL2A1). *Arthritis Rheum.* **51**, 925-932.

Marks, M. S. and Seabra, M. C. (2001). The melanosome: membrane dynamics in black and white. *Nat. Rev. Mol. Cell Biol.* **2**, 738-748.

Melville, D. B. and Knapik, E. W. (2011). Traffic jams in fish bones: ER-to-Golgi protein transport during zebrafish development. *Cell Adh. Migr.* **5**, 114-118.

Miller, E. A. and Barlowe, C. (2010). Regulation of coat assembly-sorting things out at the ER. *Curr. Opin. Cell Biol.* **22**, 447-453.

Montero-Balaguer, M., Lang, M. R., Sachdev, S. W., Knappmeyer, C., Stewart, R. A., De La Guardia, A., Hatzopoulos, A. K. and Knapik, E. W. (2006). The mother superior mutation ablates foxd3 activity in neural crest progenitor cells and depletes neural crest derivatives in zebrafish. *Dev. Dyn.* **235**, 3199-3212.

Müller, I. I., Knapik, E. W. and Hatzopoulos, A. K. (2006). Expression of the protein related to Dan and Cerberus gene–*prdc*–During eye, pharyngeal arch, somite, and swim bladder development in zebrafish. *Dev. Dyn.* **235**, 2881-2888.

Neuhauss, S. C., Solnica-Krezel, L., Schier, A. F., Zwartkruis, F., Stemple, D. L., Malicki, J., Abdelilah, S., Stainier, D. Y. and Driever, W. (1996). Mutations affecting craniofacial development in zebrafish. *Development* **123**, 357-367.

O'Donnell, J., Maddox, K. and Stagg, S. (2010). The structure of a COPII tubule. *J. Struct. Biol.* **173**, 358-364.

Rauch, F. and Glorieux, F. H. (2004). Osteogenesis imperfecta. *Lancet* **363**, 1377-1385.

Riley, P. A., Sawyer, B. and Wolf, M. A. (1975). The melanocytotoxic action of 4-hydroxyanisole. *J. Invest. Dermatol.* **64**, 86-89.

Routledge, K. E., Gupta, V. and Balch, W. E. (2010). Emergent properties of proteostasis-COPII coupled systems in human health and disease. *Mol. Membr. Biol.* **27**, 385-397.

Sachdev, S. W., Dietz, U. H., Oshima, Y., Lang, M. R., Knapik, E. W., Hiraki, Y. and Shukunami, C. (2001). Sequence analysis of zebrafish chondromodulin-1 and expression profile in the notochord and chondrogenic regions during cartilage morphogenesis. *Mech. Dev.* **105**, 157-162.

Saito, A., Hino, S., Murakami, T., Kanemoto, S., Kondo, S., Saitoh, M., Nishimura, R., Yoneda, T., Furuichi, T., Ikegawa, S. et al. (2009). Regulation of endoplasmic reticulum stress response by a BBF2H7-mediated Sec23a pathway is essential for chondrogenesis. *Nat. Cell Biol.* **11**, 1197-1204.

Saitou, N. and Nei, M. (1987). The neighbor-joining method: a new method for reconstructing phylogenetic trees. *Mol. Biol. Evol.* **4**, 406-425.

Sarmah, S., Barrallo-Gimeno, A., Melville, D. B., Topczewski, J., Solnica-Krezel, L. and Knapik, E. W. (2010). Sec24D-dependent transport of extracellular matrix proteins is required for zebrafish skeletal morphogenesis. *PLoS ONE* **5**, e10367.

Schonthaler, H. B., Lampert, J. M., von Lintig, J., Schwarz, H., Geisler, R. and Neuhauss, S. C. F. (2005). A mutation in the silver gene leads to defects in melanosome biogenesis and alterations in the visual system in the zebrafish mutant fading vision. *Dev. Biol.* **284**, 421-436.

Schwarz, K., Iolascon, A., Verissimo, F., Trede, N. S., Horsley, W., Chen, W., Paw, B. H., Hopfner, K.-P., Holzmann, K., Russo, R. et al. (2009). Mutations affecting the secretory COPII coat component SEC23B cause congenital dyserythropoietic anemia type II. *Nat. Genet.* **41**, 936-940.

Scott, A. and Stemple, D. L. (2005). Zebrafish notochordal basement membrane: signaling and structure. *Curr. Top. Dev. Biol.* **65**, 229-253.

Seidah, N. G., Mowla, S. J., Hamelin, J., Mamarbachi, A. M., Benjannet, S., Touré, B. B., Basak, A., Munzer, J. S., Marcinkiewicz, J., Zhong, M. et al. (1999). Mammalian subtilisin/kexin isozyme SKI-1: a widely expressed proprotein convertase with a unique cleavage specificity and cellular localization. *Proc. Natl. Acad. Sci. USA* **96**, 1321-1326.

Stagg, S. M., LaPointe, P., Razvi, A., Gürkan, C., Potter, C. S., Carragher, B. and Balch, W. E. (2008). Structural basis for cargo regulation of COPII coat assembly. *Cell* **134**, 474-484.

Stephens, D. J. and Pepperkok, R. (2002). Imaging of procollagen transport reveals COPI-dependent cargo sorting during ER-to-Golgi transport in mammalian cells. *J. Cell Sci.* **115**, 1149-1160.

Storlazzi, C. T., Mertens, F., Nascimento, A., Isaksson, M., Wejde, J., Brosjo, O., Mandahl, N. and Panagopoulos, I. (2003). Fusion of the FUS and BBF2H7 genes in low grade fibromyxoid sarcoma. *Hum. Mol. Genet.* **12**, 2349-2358.

Tabas, I. and Ron, D. (2011). Integrating the mechanisms of apoptosis induced by endoplasmic reticulum stress. *Nat. Cell Biol.* **13**, 184-190.

Theos, A. C., Truschel, S. T., Raposo, G. and Marks, M. S. (2005). The Silver locus product Pmel17/gp100/Silv/ME20: controversial in name and in function. *Pigment Cell Res.* **18**, 322-336.

Theos, A. C., Berson, J. F., Theos, S. C., Herman, K. E., Harper, D. C., Tenza, D., Sviderskaya, E. V., Lamoreux, M. L., Bennett, D. C., Raposo, G. et al. (2006). Dual loss of ER export and endocytic signals with altered melanosome morphology in the silver mutation of Pmel17. *Mol. Biol. Cell* **17**, 3598-3612.

Timpl, R. and Brown, J. C. (1996). Supramolecular assembly of basement membranes. *BioEssays* **18**, 123-132.

Trojanowska, M., Carwile LeRoy, E., Eckes, B. and Krieg, T. (1998). Pathogenesis of fibrosis: type 1 collagen and the skin. *J. Mol. Med.* **76**, 266-274.

Vinson, C. R., Sigler, P. B. and McKnight, S. L. (1989). Scissors-grip model for DNA recognition by a family of leucine zipper proteins. *Science* **246**, 911-916.

Wendeler, M. W., Paccaud, J.-P. and Hauri, H.-P. (2007). Role of Sec24 isoforms in selective export of membrane proteins from the endoplasmic reticulum. *EMBO Rep.* **8**, 258-264.